Supplementary Information

Towards Nickel-Titanium Shape Memory Alloys for coatingless icephobic materials

Luca Stendardo[1,2], Francesca Villa[2], Davide Parlato[1], Riccardo Motto[1], Mauro Mameli[3], Carlo Antonini[1,*], Paola Bassani[2,*]

[1]Department of Materials Science, University of Milano - Bicocca, Milano, Italy

[2]National Research Council of Italy, Institute of Condensed Matter Chemistry and Technologies for Energy, CNR ICMATE, Unit of Lecco, Via Previati 1/E, 23900 Lecco, Italy

[3]Department of Energy, Systems Land and Construction Engineering, University of Pisa, L. Lazzarino, Pisa, Italy

* corresponding authors:

Carlo Antonini: carlo.antonini@unimib.it

Paola Bassani: paola.bassani@cnr.it

KEYWORDS: Nickel Titanium, Ice adhesion, characterization, icephobic, durable

1 Section S1. 3D profilometer images

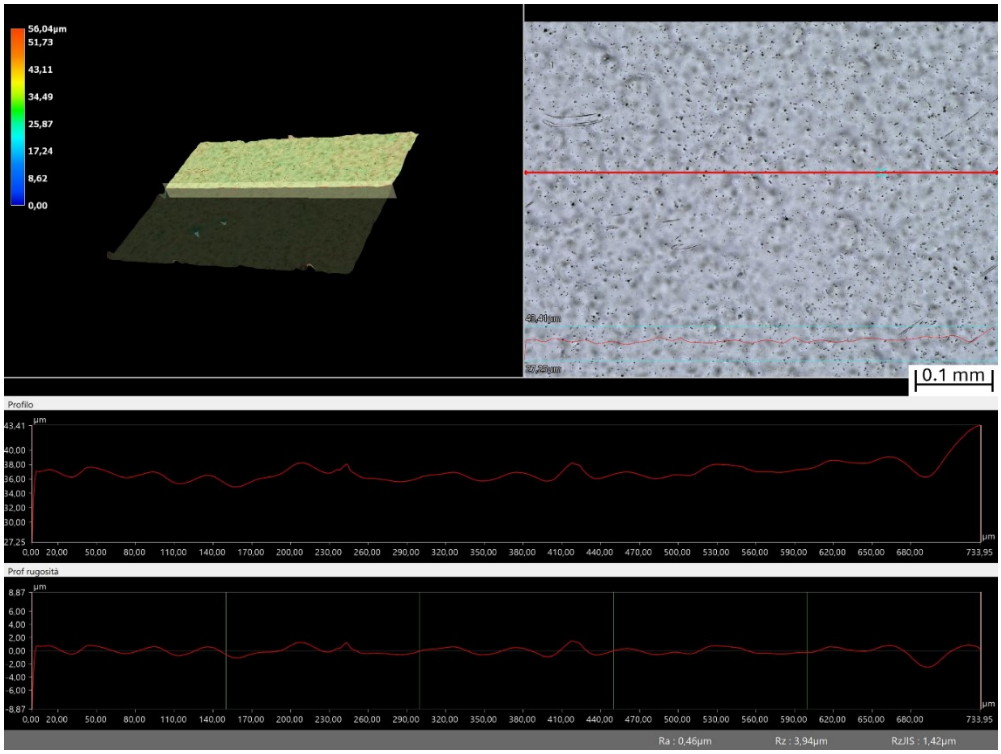

Figure S 1: 3D optical profilometer data of the electropolished (EP) sample including height profile rendering, optical image, and roughness profiles.

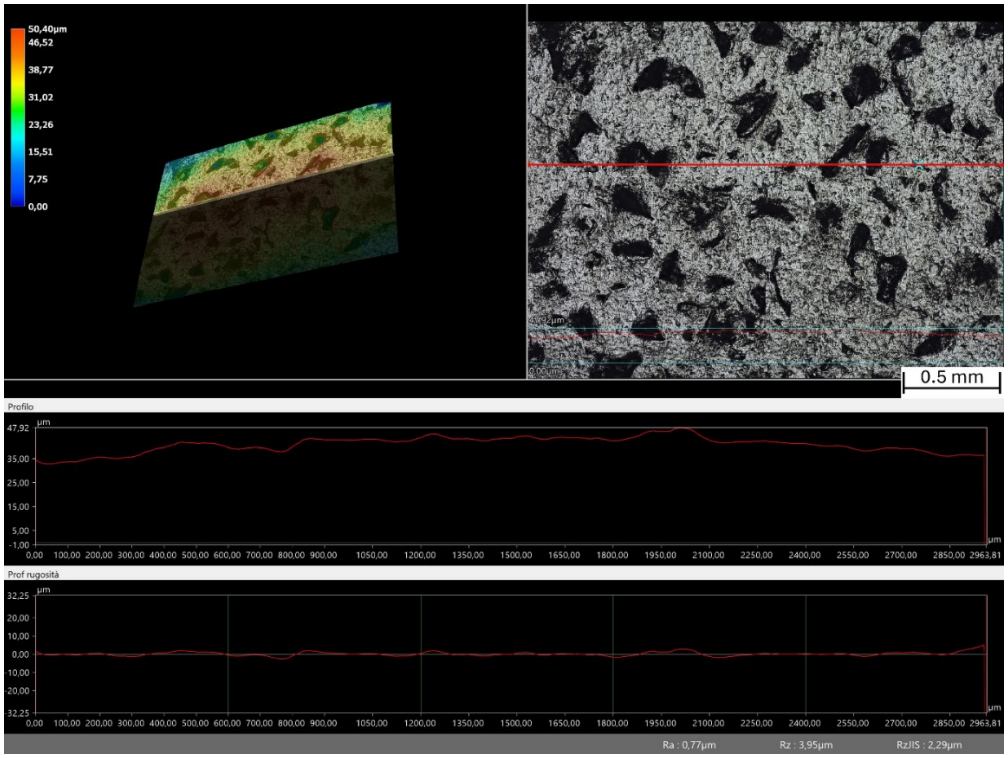

Figure S 2: 3D optical profilometer data of the 60-grit pressed (Pr. P60) sample including height profile rendering, optical image, and roughness profiles.

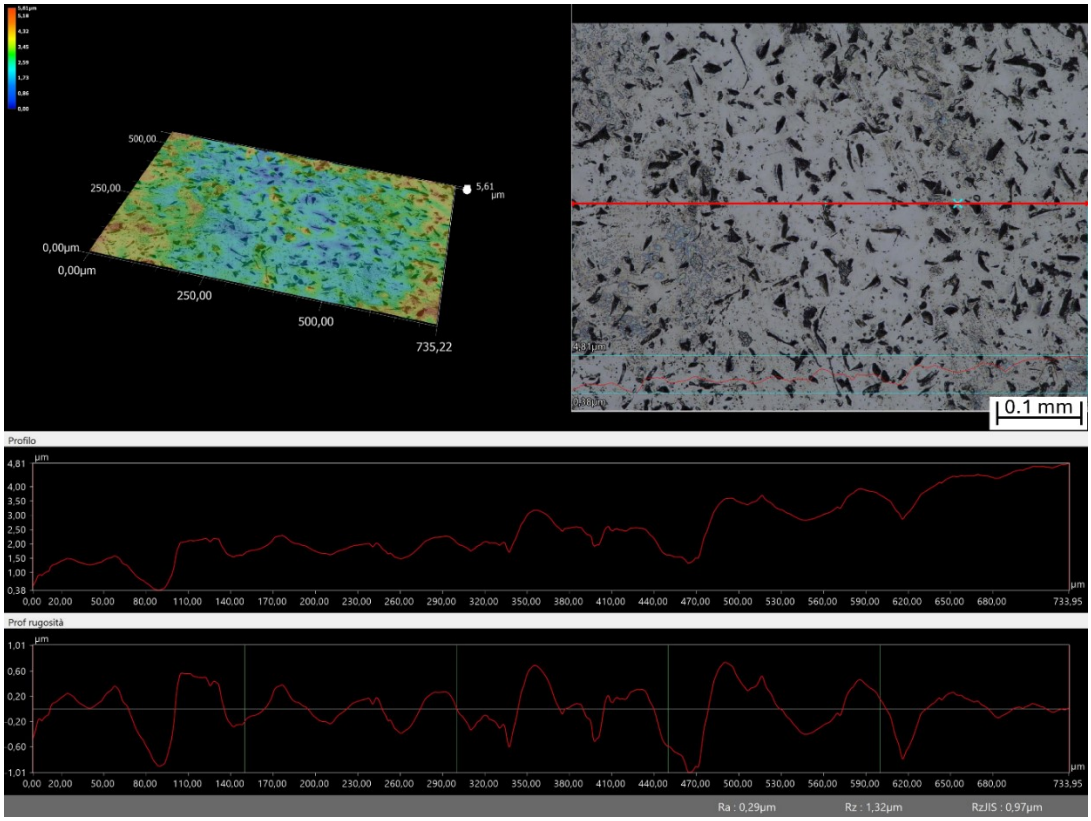

Figure S 3: 3D optical profilometer data of the 600-grit pressed (Pr. P600) sample including height profile rendering, optical image, and roughness profiles.

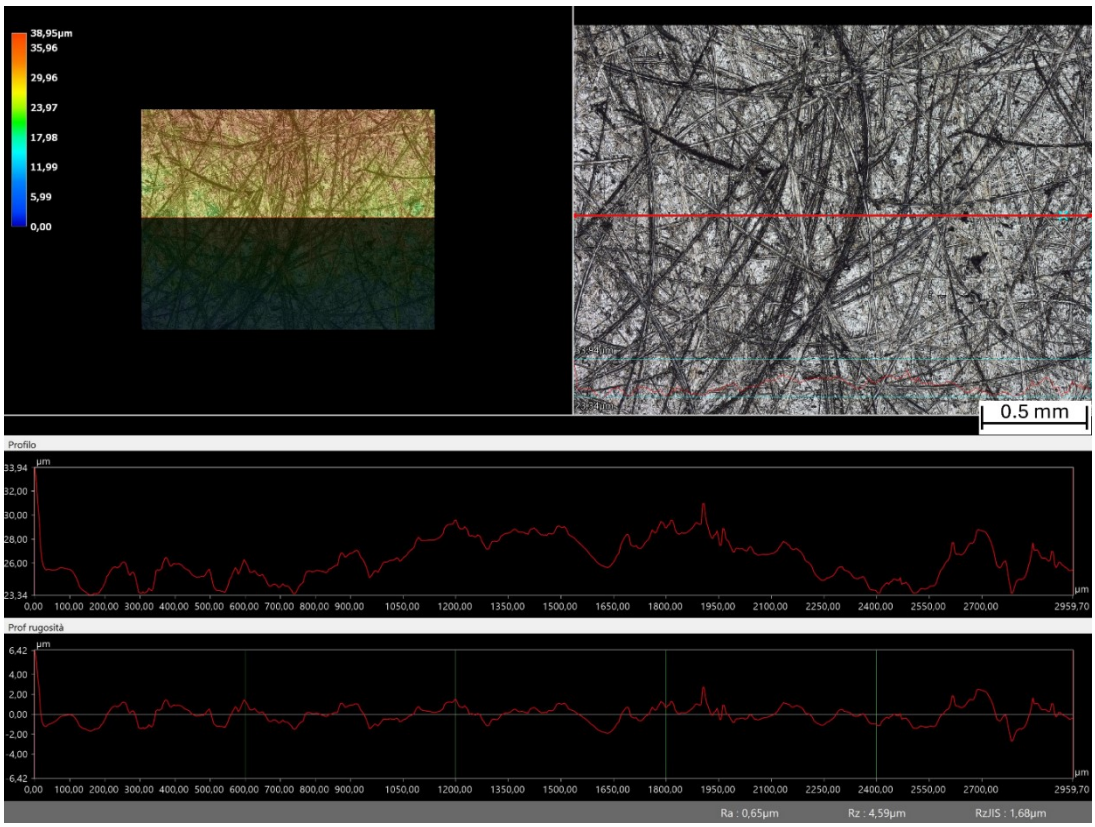

Figure S 4: 3D optical profilometer data of the 60-grit abraded (Abr. P60) sample including height profile rendering, optical image, and roughness profiles.

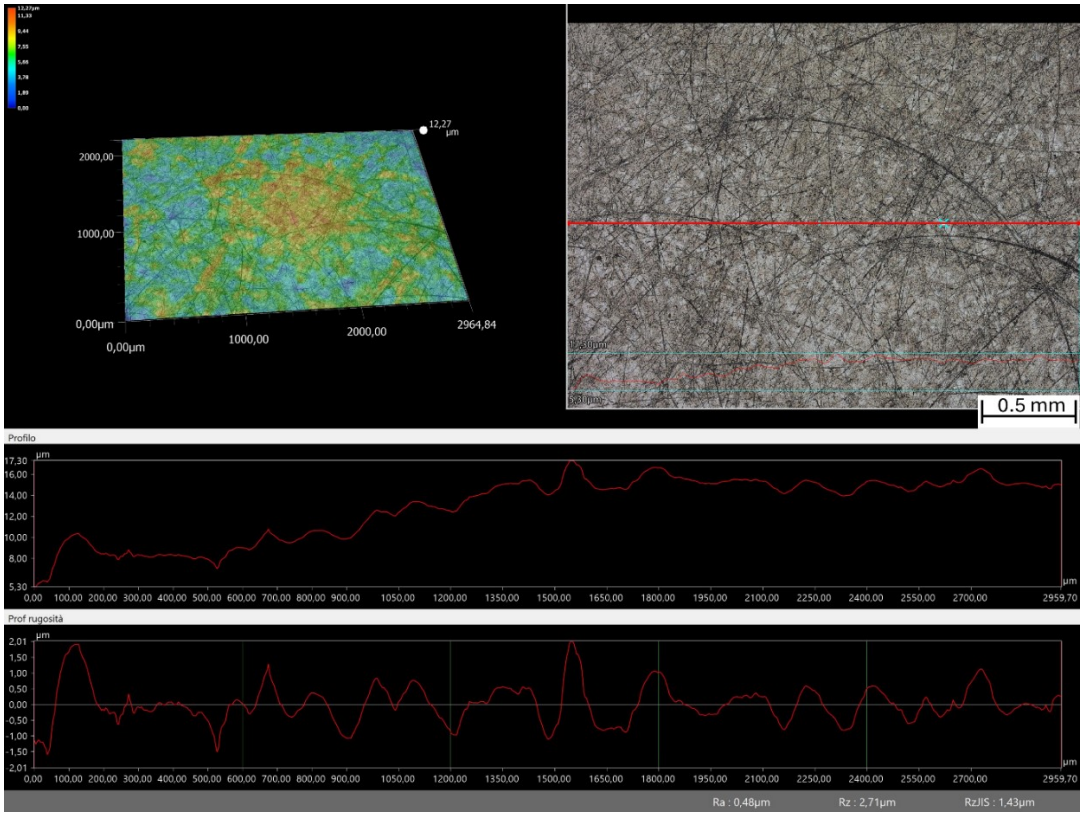

33

34 Figure S 5: 3D optical profilometer data of the 600-grit abraded sample (Abr. P600) sample including height
35 profile rendering, optical image, and roughness profiles.

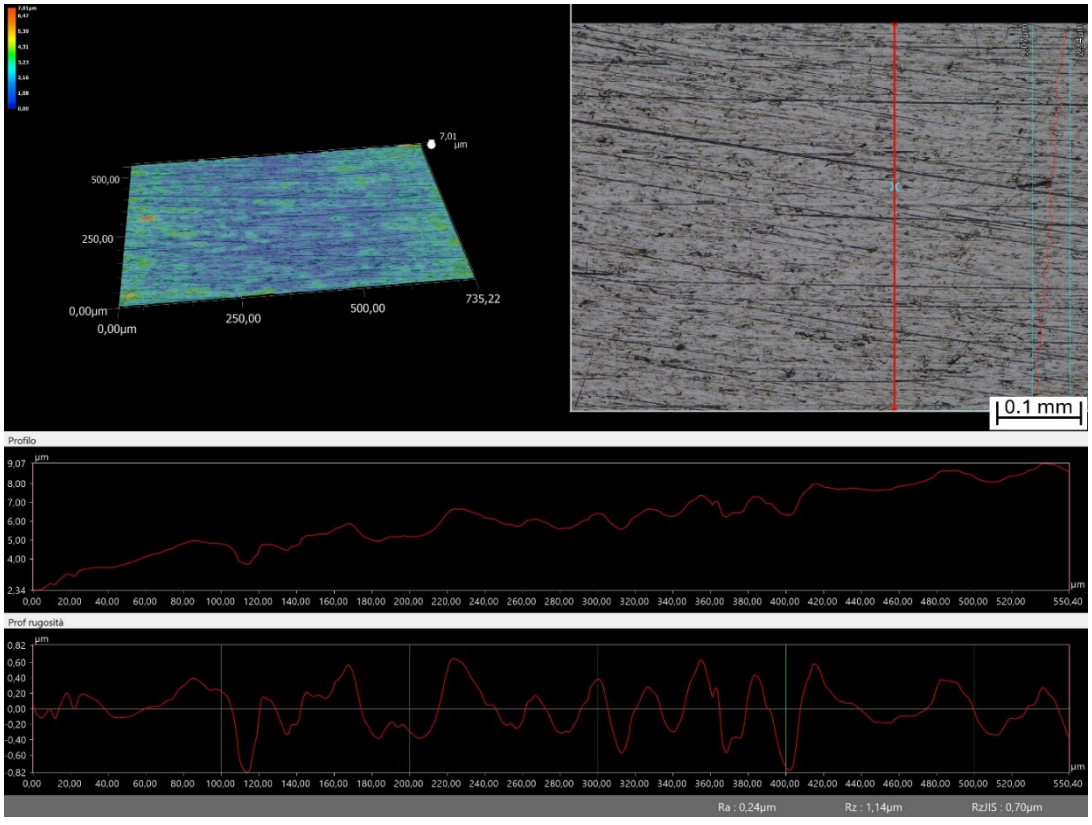

36

37 Figure S 6: 3D optical profilometer data of the 1200-grit abraded NiTi sample of 0.2 mm thichness, including
38 height profile rendering, optical image, and roughness profiles.

2 Section S2. Dynamic contact angle for NiTi samples of 0.2 mm and 1 mm thickness

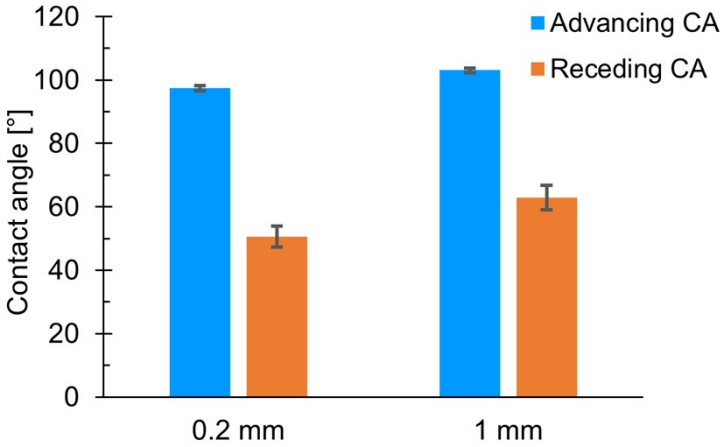

Figure S 7: Advancing and receding contact angle (CA) of the NiTi samples of 0.2 mm and 1 mm thickness, respectively. Both samples have been superficially abraded with grit 1200 SiC paper.

3 Section S3. Stress-Strain graphs of the tensile tests

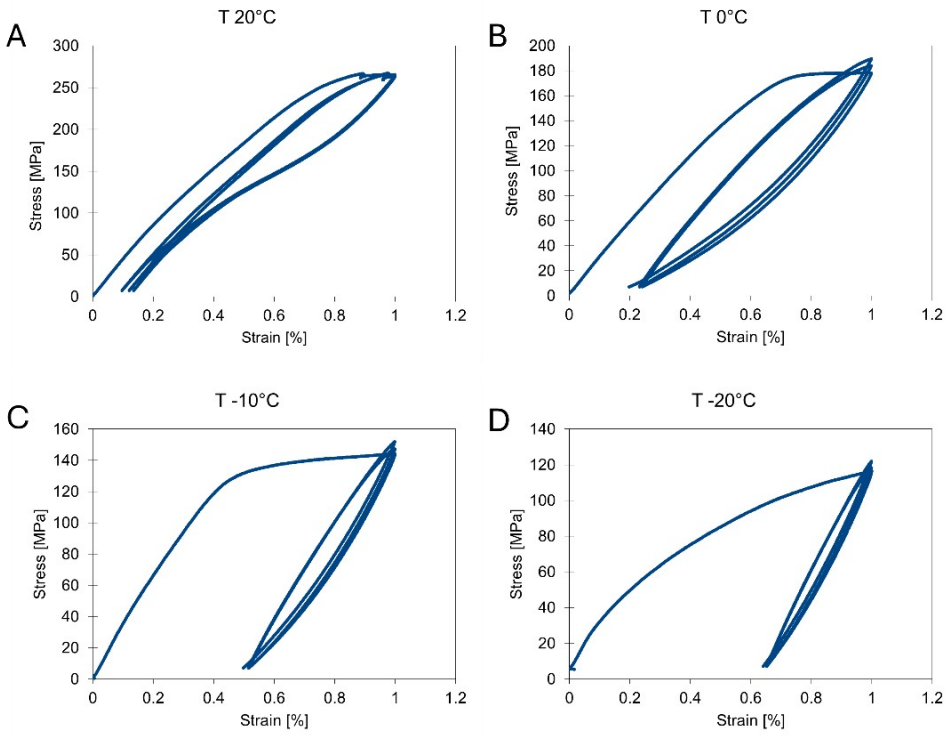

Figure S 8: Stress-Strain graphs of the NiTi alloy used for the preparation of the grit-1200 samples of 0.2 mm thickness. The tests have been carried out at different temperatures, (A) at ambient temperature (20°C), (B) at 0°C, (C) at -10°C, and (D) at -20°C.

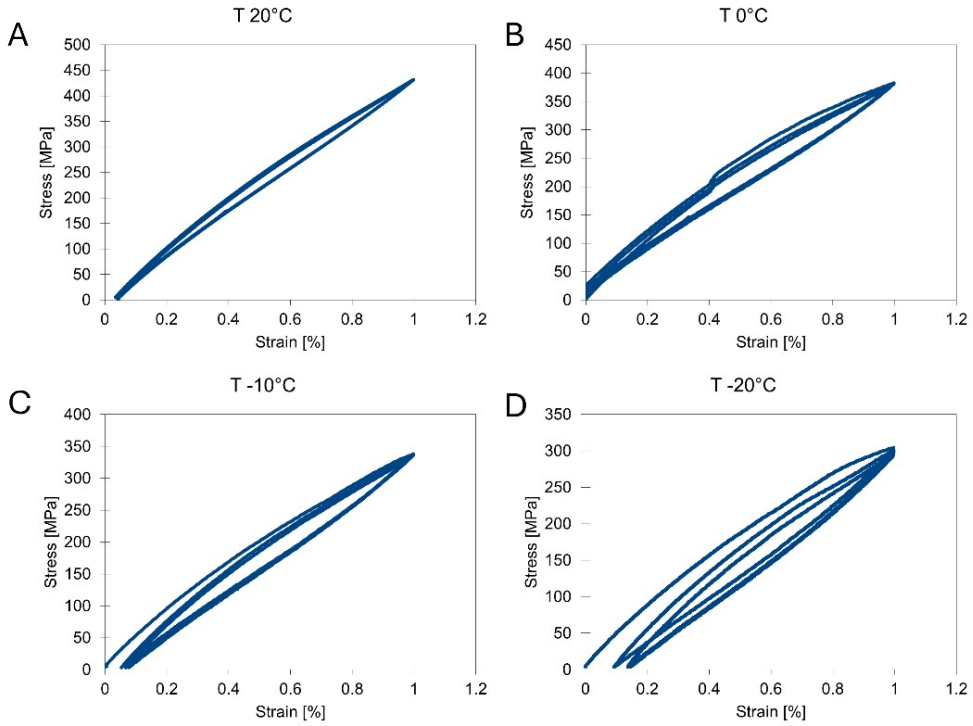

Figure S 9: Stress-Strain graphs of the NiTi alloy used for the preparation of the grit-1200 samples of 1 mm thickness. The tests have been carried out at different temperatures, (A) at ambient temperature (20°C), (B) at 0°C, (C) at -10°C, and (D) at -20°C.

4 Section S4. Theoretical fracture mechanics framework

An interfacial fracture mechanism characterized by a complete and instantaneous rupture is dominated by stress and can be described according to the following equations:

$$\tau \geq \tau_c, \forall x \in S \quad , \tag{1}$$

or, if the tensile stress is dominant,

$$\sigma \geq \sigma_c, \forall x \in S, \tag{2}$$

where the location on the interface is indicated by x and the interface by S. This fracture pattern is typically observed in ice layers characterized by uniform stress distribution at the ice-substrate interface, in the absence of significant stress concentrations. Such conditions are generally achieved in ice formations with short dimensions and substantial thickness.

For this type of fracture, critical stress threshold needs to be reached in every point of the interface in order to achieve detachment, and, therefore, the minimum stress values, τ_{min} or σ_{min}, represent the critical stress values (see Equations (1) and (2)). Conventional ice adhesion testing methods, including horizontal shear tests, generally measure the maximum force required for ice removal F_{max} and utilize this value to determine the average adhesion strength

through $\tau_{ave} = F_{max}/A$, where A represents the ice-substrate interfacial area. It is important to recognize that this average shear stress τ_{ave} does not constitute a pure surface property, but rather depends on multiple geometric factors, including ice block geometry and loading configuration. To achieve an accurate characterization of adhesion strength as an intrinsic surface property, τ_{min} must be derived from the measured τ_{ave} values. This derivation is system specific and is described in detail in Section 2.3 of the main text.

Under conditions of high stress concentrations and thin ice layers, toughness-dominated fracture mechanisms prevail. Crack propagation and ice detachment are controlled by strain energy (or interfacial toughness) rather than stress. In this regime, toughness represents the interface resistance to crack growth, or the maximum strain energy that can be stored before joint failure. Higher toughness values require greater strain energy for crack propagation.

This fracture mechanism initiates near stress concentration points. Crack formation begins with a finite opening area ΔS between the ice and substrate, representing partial separation since ΔS remains smaller than the total interface area S. The occurrence of this initial opening requires both stress and strain energy to simultaneously reach their critical thresholds, a condition named the "coupled criterion":

$$\tau \geq \tau_c, \forall x \in \Delta S \tag{3}$$

$$-\Delta W_p \geq G_c \Delta S \tag{4}$$

where G_c represents the interfacial toughness, and $-\Delta W_p = W_p(0) - W_p(S)$ indicates the potential strain energy change between the intact state and the state after initial opening. Following crack initiation, ice-substrate separation is governed exclusively by interfacial toughness.

The mechanism governing crack advancement along the interface after the initial opening can be explained using Griffith's energy-based approach. Here, crack advancement by ∂S along the interface produces a corresponding change in potential strain energy ∂W_p. The differential energy release rate can therefore be defined as:

$$-\frac{\partial W_p}{\partial S} = G \geq G_c \tag{5}$$

For every incremental crack surface area, the condition $G \geq G_c$ must hold.

The presence of two different fracture mechanisms demonstrates that ice adhesion requires more than one parameter for complete characterization, contrary to the common literature practice of using solely $\tau_{ave} = F/A$. Ice adhesion can be quantified in stress units (Pa) only when detachment follows a stress-dominated mode. In toughness-controlled fractures, strain energy (J) governs ice detachment, rendering the concept of average adhesion strength inappropriate.

5 Section S5. Ice detachment forces

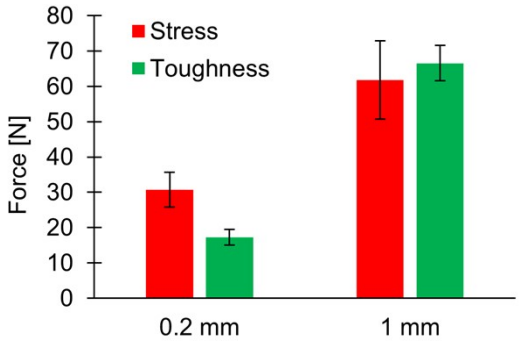

Figure S 10: Forces measured to detach the ice for both grit-1200 NiTi samples of thickness 0.2 mm and 1 mm. The forces for stress- and toughness-dominated ice detachment are reported for both samples.

6 Section S6. Ice Adhesion vs. Ra 3D, Sa 3D, and Contact Angle

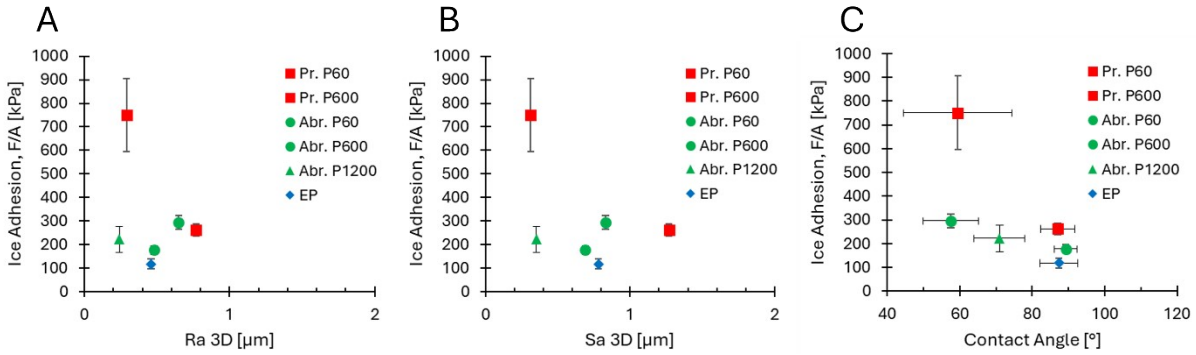

Figure S 11: Correlation between ice adhesion values and (A) Ra 3D, (B) Sa 3D, and (C) Contact angle. In all three cases, a lack of one-to-one correlation was observed.

7 Section S7. SEM images of the samples

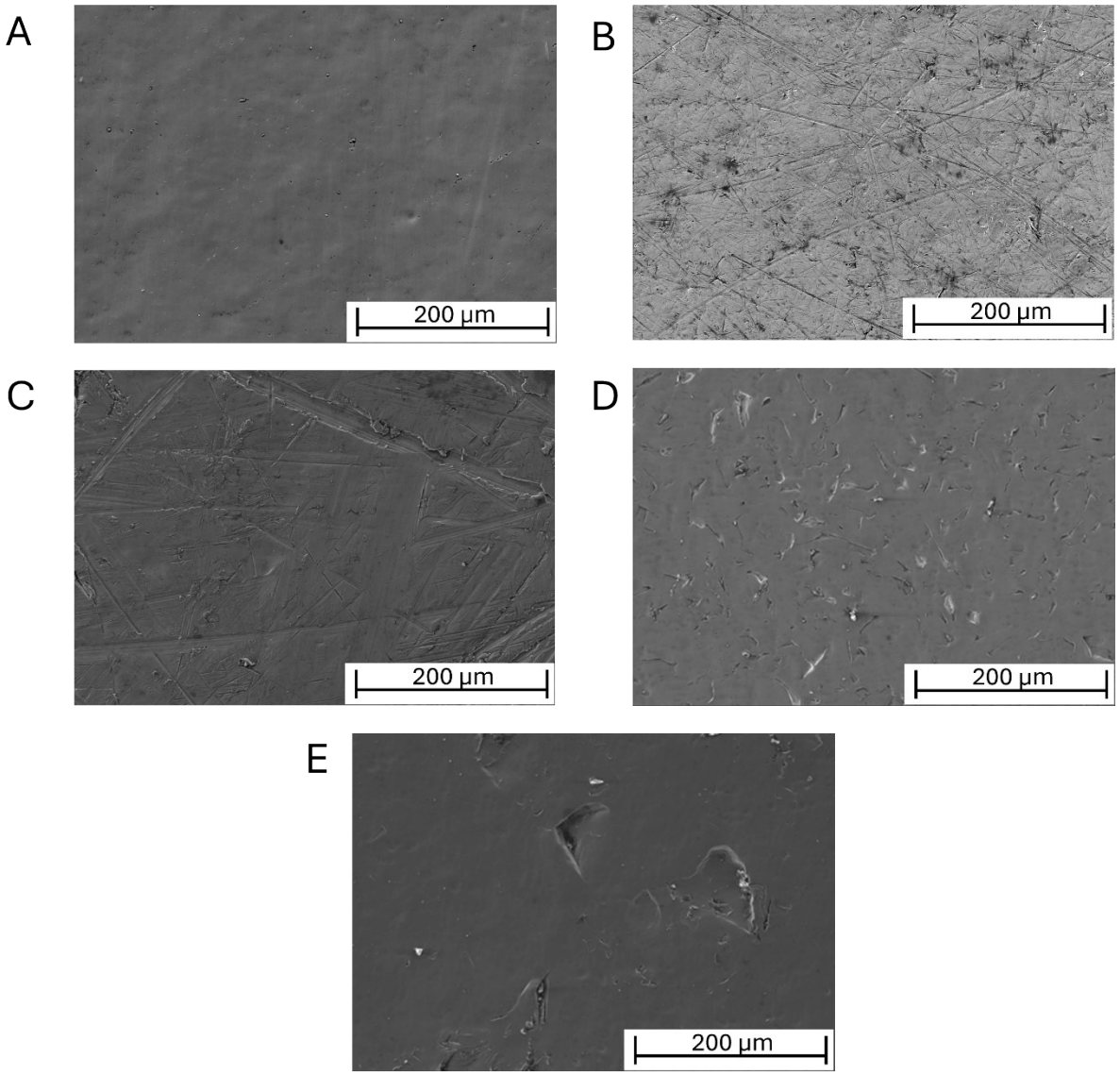

Figure S 12: SEM images of the samples (A) EP, (B) Abr. P600, (C) Abr. P60, (D) Pr. P600, and (E) Pr. P60.

8 Section S8. Surface feature distance and size measurements

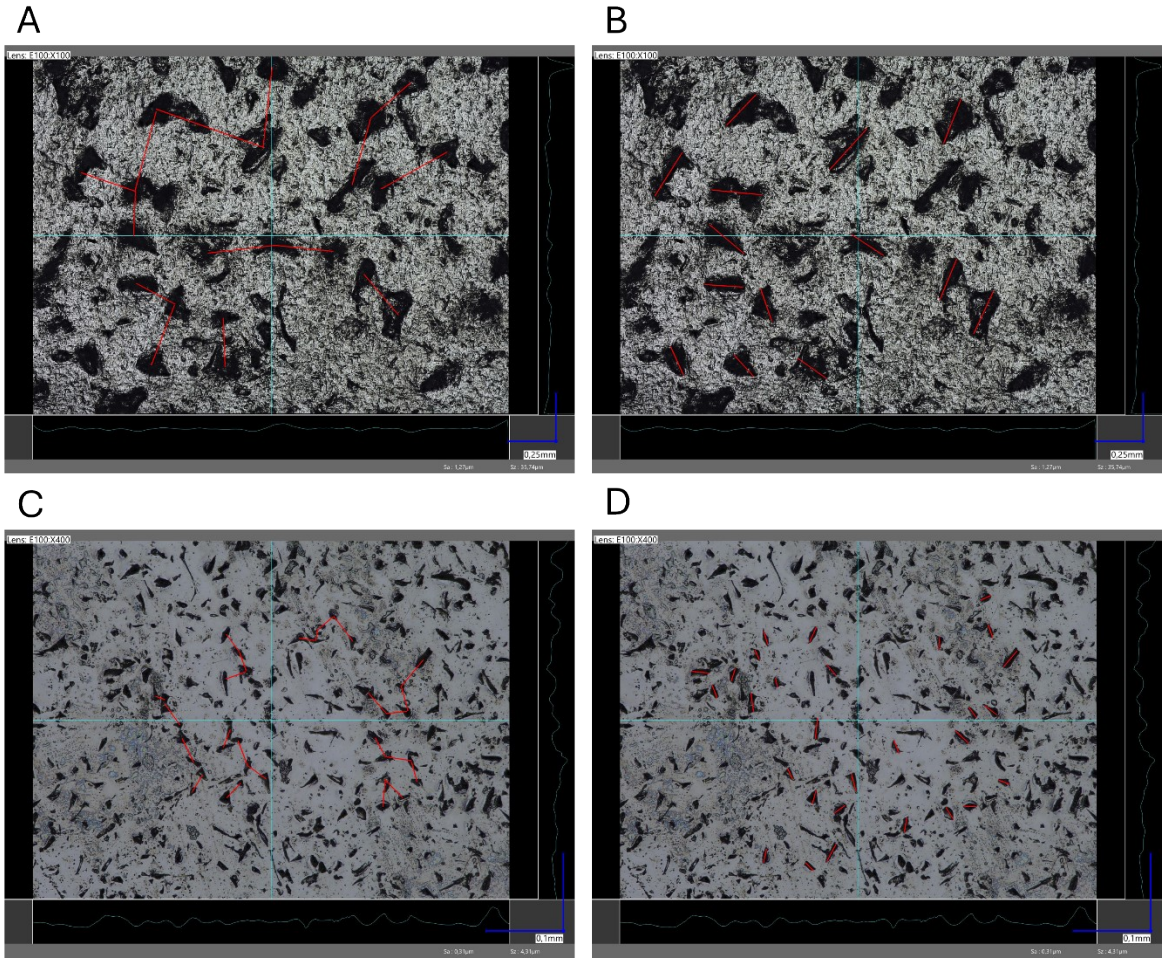

Figure S 13: Red line segments indicate the measurements on the samples Pr. P60 (A and B) and Pr. P600 (B and C). The distances between surface features were measured in (A) and (C), the size of the individual features were measured in (B) and (D).

9 Section S9. Differential scanning calorimetry (DSC) analysis of the NiTi alloys

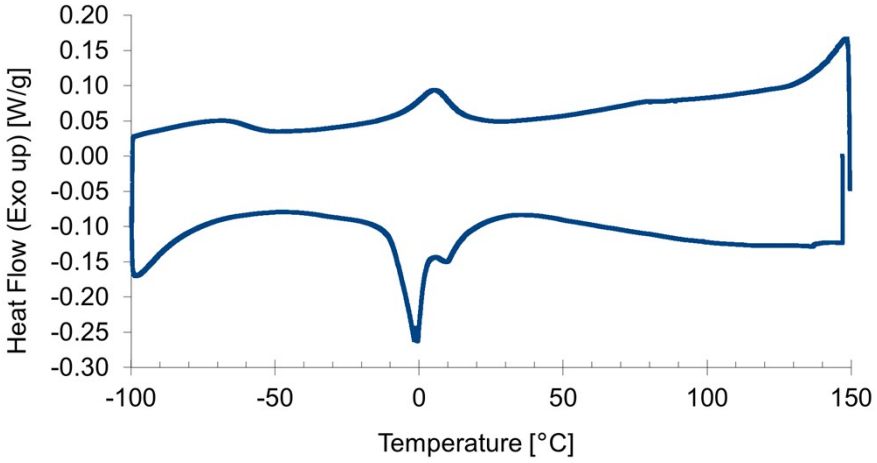

Figure S 14: DSC analysis of the NiTi alloy used for the preparation of the grit-1200 samples of 0.2 mm thickness.

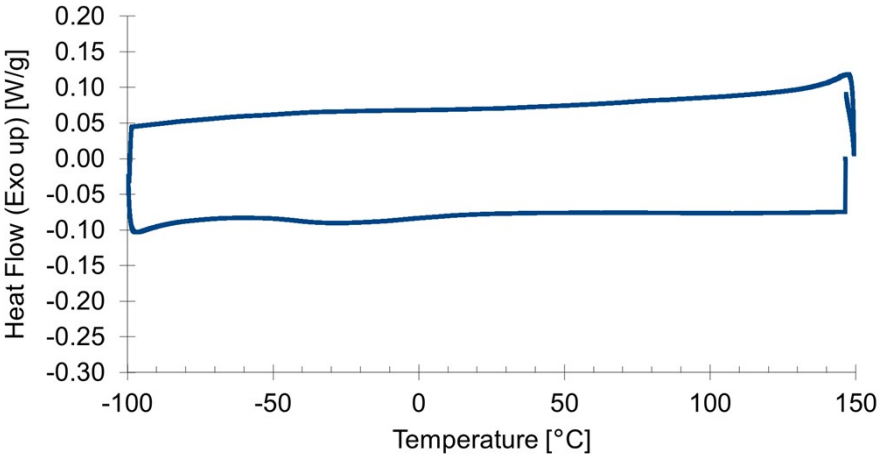

Figure S 15: DSC analysis of the NiTi alloy used for the preparation of the grit-1200 samples of 1 mm thickness.